Title

Signal scaling improves the signal-to-noise ratio of measurements with segmented 2D-selective radiofrequency excitations

Journal

Magnetic Resonance in Medicine, 70(6)

ISSN

0740-3194

Authors

Finsterbusch, Jürgen
Busch, Martin G
Larson, Peder EZ

Publication Date

2013-12-01

DOI

10.1002/mrm.24610

Peer reviewed

HHS Public Access

Author manuscript

Magn Reson Med. Author manuscript; available in PMC 2016 August 16.

Published in final edited form as:

Magn Reson Med. 2013 December ; 70(6): 1491–1499. doi:10.1002/mrm.24610.

Signal Scaling Improves the Signal-to-Noise Ratio of Measurements with Segmented 2D-Selective Radiofrequency Excitations

Jürgen Finsterbusch[1,2,*], **Martin G. Busch**[1,2], and **Peder E. Z. Larson**[3]

[1]Department of Systems Neuroscience, University Medical Center Hamburg—Eppendorf, Hamburg, Germany

[2]Neuroimage Nord, University Medical Centers Hamburg–Kiel–Lübeck, Hamburg, Germany

[3]Department of Radiology and Biomedical Imaging, University of California—San Francisco, San Francisco, California, USA

Abstract

Purpose—Segmented 2D-selective radiofrequency excitations can be used to acquire irregularly shaped target regions, e.g., in single-voxel MR spectroscopy, without involving excessive radiofrequency pulse durations. However, segments covering only outer k-space regions nominally use reduced B1 amplitudes (i.e., smaller flip angles) and yield lower signal contributions, which decreases the efficiency of the measurement. The purpose of this study was to show that applying the full flip angle for all segments and scaling down the acquired signal appropriately (signal scaling) retains the desired signal amplitude but reduces the noise level accordingly and, thus, increases the signal-to-noise ratio.

Methods—The principles and improvements of signal scaling were demonstrated with MR imaging and spectroscopy experiments at 3 T for a single-line segmentation of a blipped-planar trajectory.

Results—The observed signal-to-noise ration gain depended on the 2D-selective radiofrequency excitation's resolution, field-of-excitation, and its excitation profile and was between 40 and 500% for typical acquisition parameters.

Conclusion—Signal scaling can further improve the performance of measurements with segmented 2D-selective radiofrequency excitations, e.g., for MR spectroscopy of anatomically defined voxels.

Keywords

2D-selective RF excitations; segmentation; signal scaling; noise reduction; single-voxel MR spectroscopy

[*]Correspondence to: Jürgen Finsterbusch, Ph.D., Institut für Systemische Neurowissenschaften, Geb. W34, Universitätsklinikum Hamburg-Eppendorf, 20246 Hamburg, Germany. j.finsterbusch@uke.uni-hamburg.de.

INTRODUCTION

Spatially 2D-selective radiofrequency (2DRF) excitations are able to excite arbitrarily shaped profiles within the plane defined by their trajectory (1–3). This capability can be used, for instance, to image curved slices (e.g., (4)) and inner fields-of-view (e.g., (5–7)) without aliasing artifacts in the phase encoding direction, to compensate B_1 inhomogeneities (e.g., Ref. 8), and to minimize partial volume effects in MR spectroscopy (MRS) by acquiring tailored voxels (e.g., (9–11)). In particular for the latter application, the desired profile should be realized with a high spatial resolution, i.e., a good profile sharpness. However, corresponding 2DRF excitations may require long pulse durations and can have a pronounced sensitivity to relaxation effects, magnetic field inhomogeneities, and chemical shifts.

To reduce this sensitivity and avoid excessive 2DRF pulse durations, segmentation can be used (e.g., (12,13)). Thereby, the full 2DRF excitation is split into several, short sections that are applied in successive acquisitions. Averaging the complex signals of all segments then yields the desired excitation profile. However, some of the segments may cover only outer k-space regions, e.g., when using a blipped-planar trajectory. These segments have a lower nominal flip angle compared with the segment(s) covering the k-space center and, thus, provide only small signal contributions, which decreases the signal efficiency significantly (e.g., Ref. 14). In the case averaging is performed, like in single-voxel MRS, the efficiency can be improved significantly by applying weighted averaging with flip angle adaptation (15). But for a typical number of averages, the flip angles of some or many segments will remain reduced yielding a nonoptimum efficiency (15).

In this study, it is shown that the efficiency of the measurement, i.e., its signal-to-noise ratio (SNR), can be further increased by using a signal scaling approach. The full flip angle is used for all segments, and prior to averaging, the signals are scaled down to obtain the desired signal amplitude. This upscaling of the flip angle and downscaling of the acquired signal reduces the acquired noise, i.e., increases the SNR. This is demonstrated for single-voxel MRS of tailored target volumes in the human brain in vivo.

Principles

2DRF excitations based on a single-line segmentation of a blipped-planar trajectory are used to demonstrate the crucial advantage of the proposed signal scaling (see Fig. 1). For this trajectory, the unwanted side excitations are limited to a single direction and, thus, can be easily eliminated with a refocusing RF pulse (13,14). Furthermore, and more importantly, it provides a high bandwidth in the blip direction which minimizes chemical shift displacement artifacts (14). For clarity and simplicity, a rectangular excitation profile (Fig. 1a) was considered as an example. It yields a two-dimensional sinc function for the B_1 weighting in k-space (Fig. 1b) and sinc-shaped RF envelopes for all lines (Fig. 1c) in the low-flip-angle approximation (3). But the RF amplitude and, thus, the flip angle α_i varies for the different segments according to their relative B_1 weighting in k-space as is sketched in the adapted PRESS sequence (Fig. 1d).

In a conventional experiment, the same number of averages ($n_i = n$) is used for all segments, independent of their relative B_1 weightings and flip angles α_i. However, this is quite inefficient, as segments covering outer k-space lines provide only a small flip angle, i.e., minor signal contributions. Nevertheless, they are required to define the higher spatial frequencies of the excitation profile and realize the desired profile sharpness.

The signal efficiency can be improved by weighted averaging with flip angle adaptation (15). The number of averages for segments covering outer lines is decreased to a segment-specific value (n_i), and their flip angles are adapted (α_i'), i.e., increased accordingly, to obtain the same signal amplitude within fewer averages. The time saved can be used to increase the number of averages of the central segment that provides the highest flip angle (α_{max}) and signal amplitude. Thus, the signal efficiency can be increased considerably (15). This approach yields an optimal efficiency in the limit of many acquisitions, where the full flip angles (α_{max}) is applied for all segments, and the different weightings required for the individual segments are only reflected in their number of averages n_i (15). But otherwise, i.e., for a low or medium number of acquisitions, most segments will still have a low(er) flip angle $\alpha_i' < \alpha_{max}$ that corresponds to a reduced efficiency. This holds in particular for the minimum number of acquisitions, i.e., if the number of acquisitions is equal to the number of segments ($n_i = 1$). Then, no weighted averaging can be performed, and the approach degrades to the conventional experiment.

To increase the efficiency, a signal scaling approach can be used. It involves the application of the full flip angle for all segments, which maximizes the signal amplitude for each segment. To retain the relative weightings of the different segments and avoid profile distortions, the signals must be scaled down prior to averaging. This upscaling of the flip angle and downscaling of the acquired signal does not affect the signal amplitude but decreases the acquired noise that is independent of the segment's flip angle. Thus, the SNR can be improved considerably, as is demonstrated in Fig. 1e for the rectangular excitation profile. The signal amplitude decays toward outer segments according to their relative B_1 weightings in both experiments. But whereas the noise level does not change in the conventional experiment, it decreases considerably for the signal scaling approach yielding a significant SNR improvement for the rectangular profile that is obtained after averaging all acquisitions. Thus, the approach improves the measurements even with the minimum number of acquisitions, which is in contrast to the flip angle adaptation.

It should be noted that the nonlinear relationship between the flip angle and the signal must be considered for the scaling. For instance, scaling up the flip angle α_i of a segment to α_{max} requires scaling the acquired signal with a factor of $(\sin \alpha_i)/(\sin \alpha_{max})$. Only for lower flip angles where $\sin \alpha_i \propto \alpha_i$, the signal scaling factor becomes α_i/α_{max}, i.e., the reciprocal value of the flip angle scaling.

METHODS

Measurements were performed on a 3T whole-body MR system (TIM Trio, Siemens Healthcare, Erlangen, Germany) equipped with a 40-mT m^{-1} gradient system using a 12-channel receive-only head coil. Spherical water phantoms containing either $NiSO_4$ or

$NaC_2H_3O_2$ (0.10 M) and $LiC_3H_3O_3$ (0.10 M) for MRS experiments were investigated. Healthy volunteers were examined after they declared their informed consent.

A blipped-planar trajectory was used for the 2DRF excitations (cf. Fig. 1c). For this trajectory, the unwanted side excitations appear as periodic copies of the desired profile in the blip direction and can easily be eliminated by a refocusing RF pulse (see later). Their distance, the so-called field-of-excitation, increases with the the trajectory's sampling density in the blip direction. Isotropic resolutions between 5.0 and 1.0 mm and fields-of-excitation between 25 and 45 mm were used.

The 2DRF envelopes were calculated with the low-flip-angle approximation (3), i.e., using the Fourier transformation of the defined profile for the B_1 weighting in k-space. A Gaussian filter with an amplitude of 0.15 at the extreme k-space values on each axis was multiplied to the Fourier transformation to minimize ringing artifacts. The full 2DRF envelope was split into single-line segments to minimize chemical-shift displacement artifacts, yielding between nine and 45 segments for the chosen combinations of resolution and field-of-excitation. For the central segment, a maximum flip angle α_{max} of 50° was used.

A variable-amplitude (16–18) rather than trapezoidal line gradient pulses was applied (see Fig. 1d). During the central plateau (duration 2000 μs), the amplitude was 2.6 mT m^{-1}. Outside of this plateau, a maximum gradient amplitude of 16.2 mT m^{-1} was used that was ramped with 18.9 mT m^{-1} ms^{-1}. Thus, excessive RF peak amplitudes for the central part of the 2DRF pulse were avoided and outer parts were covered more rapidly to shorten the 2DRF pulses.

Rectangular profiles with sizes between 15 × 35 and 35 × 35 mm^2 (blip × line direction) were applied to demonstrate the basic properties of signal scaling. A profile covering parietal gray matter was used as an anatomically defined voxel for MRS acquisitions. It was determined on the basis of a T_1-weighted data set (voxel size 1.0 × 1.0 × 1.0 mm^3) with a spatial resolution of 1.0 × 1.0 mm^2. Its maximum dimensions were 35 mm in the left–right direction (blip direction) and 54 mm in the posterior–anterior direction (line direction). For all profiles, the direction of the smallest size was always chosen for the 2DRF's blip direction to reduce the field-of-excitation, i.e., the number of trajectory lines and segments.

For the rectangular profile, some combinations of 2DRF resolution, field-of-excitation, and profile size in the blip direction yielded single-line segments that cover zero crossings of the B_1 weighting (sinc) function. For instance, for the 35×35-mm^2 profile with a 2DRF resolution of 1 mm and a field-of-excitation of 45 mm, four of the 45 segments were zero crossings. Such segments have a flip angle of 0°, i.e., do not generate an MR signal, and were not applied to shorten the acquisition time. Similarly, a threshold was used for the segments of the gray matter profile. Segments that had an original flip angle as determined from the B_1 weighting below this threshold (typically 1% or less of that of the central segment) were not applied, as their contributions to the profile are marginal.

Images of the excitation profiles were acquired with a spin-echo sequence under fully relaxed conditions (pulse repetition time $>4T_1$) with an in-plane resolution of 2.0 × 2.0 mm^2 (slice thickness 20 mm) unless stated otherwise. Single-voxel spectra were measured with an

adapted PRESS (19) sequence (Fig. 1d). As in Ref. 15, the second refocusing RF pulse is applied to eliminate the unwanted side excitations that appear as periodic copies of the desired excitation profile in the blip direction. A pulse repetition time of 6 s, a echo time of 30 ms, a slice thickness of 20 mm in the phantom and 10 mm in vivo, and four preparation intervals to achieve steady-state conditions were used. One thousand and twenty-four data points were acquired in 1024 ms. In both sequences, the unwanted side excitations of the 2DRF pulse were eliminated by a refocusing RF pulse in the blip direction (see Fig. 1d). Unless stated otherwise, its width was chosen to be the profile size in the blip direction plus 5 mm and varied between 20 and 40 mm. The field-of-excitation of the 2DRF pulse was always obtained by adding another 5 mm, i.e., it usually exceeded the profile size in the blip direction by 10 mm. This setup was used to ensure that even in the presence of slice profile imperfections of the refocusing RF pulse (i) the desired excitation profile is fully refocused and (ii) the side excitations are completely eliminated.

In conventional experiments, the flip angle obtained from the B_1 weighting of each segment was applied, and an identical number of averages was used for all segments. For weighted averaging with flip angle adaptation, the number of averages was minimized for each segment, and the flip angle adapted accordingly to obtain the desired signal amplitude without exceeding the flip angle of the central segment (15). Signal scaling was implemented as an extension of this approach, i.e., weighted averaging was used (shown to be beneficial later). But the maximum rather than an adapted flip angle was used for all segments, and the acquired signals were scaled with a positive factor (≤1) to restore the required signal amplitudes.

Signal amplitudes and noise levels were determined to estimate the SNR. In the images, the signal amplitude was determined as the mean intensity in a homogeneous region of the profiles and noise levels were obtained from the mean intensity in a background region. For the spectra, the area of the largest peak as determined with LCModel (20) was used for the signal amplitude. The noise level was the standard deviation of the real component from acquisitions with all RF pulses turned off.

To evaluate the SNR improvement of signal scaling compared with flip angle adaptation over a large range of acquisitions, an IDL algorithm (version 7.1, ITT Visual Information Solutions, Boulder, CO, USA) was used. In addition to the scaling factors of the individual segments f_i, the square root of their weighted sum-of-squares, $f_{\mathrm{sum}}=\sqrt{\sum_i n_i \cdot f_i^2}$, was determined as a measure for the overall noise scaling. Accordingly, the SNR is expected to scale with $1/f_{\mathrm{sum}}$.

RESULTS

Figure 2 shows the dependency of the SNR gain for signal scaling (compared to flip angle adaptation) on the total number of acquisitions N for the 2DRF excitation of Fig. 1e. The three examples of Fig. 2a reflect the overall trend present. For only a few ($N = 9$) acquisitions, the SNR gain is quite prominent (about 200%). For a medium N (16 acquisitions), it is reduced but still significant (about 25%), whereas for a large N (64

acquisitions) only a minor SNR gain (about 3%) is present that cannot be seen with the naked eye.

In Fig. 2b, the signal scaling factors of the individual segments and their weighted average are plotted. For the central segment (segment #5), the factor is fixed to 1, because this segment has the maximum B_1 weighting. For the minimum $N = 9$, each segment is acquired only once, so the scaling factors of the other segments are determined by the relative B_1 weighting in k-space. Increasing N means that more averages are used for the central segment, so larger signal amplitudes and larger scaling factors for other segments are required to retain the relative weightings. This trend continues until a higher signal amplitude is required for a segment than could be delivered by a single average with a scaling factor of 1.0. Then, two averages are used, and the scaling factor of this segment is reduced accordingly, i.e., could be reduced to $\frac{1}{2}$, shown by the initial discontinuities in the outer segment plots. For even larger N, it increases again until a third average is necessary, which then could reduce the scaling factor to $\frac{2}{3}$ and so on. In the limit of a large N, all scaling factors approach 1, and the different B_1 weightings required are only reflected in their relative number of averages. Signal scaling is then equivalent to flip angle adaptation.

Because the scaling factors define the noise reduction with signal scaling, their weighted average f_{sum} reflects the overall decrease of the noise level compared with flip angle adaptation. From a start value of about 0.35 for $N = 9$ (which corresponds with the experimental data of Fig. 2a), it increases to almost 1 for $N > 100$. The intermediate values at $N = 16$ and $N = 64$, about 0.75 and 0.93, respectively, are also in agreement with those observed experimentally (see earlier). The exact values of the SNR gain achieved depend on the segments' B_1 weightings and, thus, on the size and shape of the excitation profile as well as the trajectory used and its parameters, as is demonstrated in Fig. 3. To increase the 2DRF resolution (Fig. 3a), additional lines in outer k-space (with low B_1 weightings) must be covered. This implies that (i) the signal amplitude remains almost unaffected, (ii) the noise level increases because more acquisitions are performed, and (iii) the averaged scaling factor decreases. Therefore, the SNR gain with signal scaling increases with finer resolution, which is clearly visible in Fig. 3a. For a resolution of 5 mm, the SNR is improved by about 200% but by about 500% for a resolution of 1 mm. This also means that the range in which a considerable improvement can be observed is shifted toward larger N for finer resolutions. This can be seen in Fig. 3b where a resolution of 1 mm was used: for 64 acquisitions, the SNR gain is about 50%, which is considerably more than the about 3% observed for a resolution of 5 mm (Fig. 2a, see earlier).

For the smallest profile size in the blip direction considered (Fig. 3c), the noise level is reduced for flip angle adaptation, because fewer acquisitions are performed (more segments cover a zero crossing and are discarded). In contrast, the noise level for signal scaling increases, because the weighting function in k-space is broadened and the B_1 weightings of outer segments are increased, which decreases their scaling factors. This means that the SNR gain of signal scaling is reduced for smaller profile sizes (from about 500% for 35 mm to about 230% for 15 mm).

Figure 3d shows that weighted averaging is beneficial for signal scaling, i.e., it is advantageous to minimize the number of averages for each segment. For 82 acquisitions, the SNR is increased by about 20% for weighted averaging compared with conventional averaging.

Figure 4 shows an anatomically defined 2D target profile that was derived from the shape of the gray matter in a healthy volunteer (Fig. 4a), and corresponding excitation profiles created in a uniform phantom (Fig. 4b). For signal scaling, some minor reduction of the signal amplitude was observed (about 5% compared with the conventional approach), but the noise level was reduced by about 80%, i.e., the SNR was increased by about 370%. In Fig. 4c, the effect of discarding segments with small B_1 weightings is shown. For thresholds (relative to peak B_1 weighting) of 0.50% and above, a difference compared with the acquisition with all segments is clearly present. But for the lower thresholds, the deviation is marginal, e.g., the peak difference for a threshold of 0.25% was only twice the peak intensity in a background noise region. Thus, the contributions of the thresholded segments can be considered to be negligible, and a threshold of 0.25% was used for all other acquisitions with the gray matter profile. This reduced the number of segments from 45 to 39 without affecting the signal amplitude.

Figure 5 summarizes the results of single-voxel MRS acquisitions that were performed with typical numbers of acquisitions (64 and 68). The reduced noise level with signal scaling can be clearly seen in the amplified noise part of the spectrum and the extra noise acquisitions, respectively. The SNR increase was estimated to be about 65% for the rectangular profile, and about 55 and 60% for the gray matter profile in the phantom and in vivo, respectively.

DISCUSSION

In signal scaling, the full flip angle is applied for all segments of a 2DRF excitation, independent of their B_1 weighting. To restore the relative signal amplitudes that are required to realize the desired profile without distortions, the acquired signal must be scaled accordingly. Although upscaling the flip angle and downscaling the acquired signal does not affect the relevant signal amplitude, the noise level that is independent of the flip angle is reduced correspondingly, which ultimately improves the SNR. This has been demonstrated in phantom and in vivo measurements for a single-line segmentation of a blipped-planar trajectory targeting tailored MRS voxels.

Signal scaling performs better with weighted averaging (15) as compared to conventional averaging. It involves minimizing the number of averages for each segment and increasing the scaling factor appropriately. The saved time can be used to increase the number of averages of the central segment accordingly. This elevates the noise level but increases the signal amplitude much more yielding a higher SNR.

But weighted averaging also improves the flexibility. In conventional averaging, the total number of averages must be a multiple of the number of segments, e.g., 39 for the used gray matter profile. With weighted averaging, the number of acquisitions can be increased

arbitrarily (15), e.g., yielding 39, 40, 45, and 46 acquisitions with one, two, three, and four averages of the central segment, respectively.

The SNR gain achieved for signal scaling compared with flip angle adaptation depends not only on the profile size and shape but also on the trajectory and its segmentation scheme. Of particular importance is the number of acquisitions performed for all segments and the number of segments that cover solely outer k-space regions with a low B_1 weighting. Such segments benefit considerably from signal scaling, if only a low or medium number of acquisitions can be used. In particular, signal scaling also improves measurements with the minimum number of acquisitions, which is in contrast to flip angle adaptation. In the limit of many acquisitions, signal scaling and flip angle adaptation become equivalent, but the SNR remains considerably improved compared with conventional averaging.

The single-line segmentation of a blipped-planar trajectory (14) that has been used in this study benefits notably from signal scaling, because it provides many segments covering solely outer k-space lines. Similarly, trajectories covering S-shaped curves on different spherical shells that have been used for single-voxel MRS with 3D-selective RF excitations (11) can be expected to profit considerably from signal scaling and weighted averaging. The improvement for trajectories that cover the k-space center with many or even each segment can be expected to be less pronounced but could be still relevant. Due to the high sampling density in the k-space center that requires a reduction of its relative weighting (21), the different contributions of outer regions may cause a flip angle variation across the segments that is the basis for an SNR improvement with signal scaling.

Care must be taken for acquisitions with arbitrarily shaped excitation profiles, if short repetition times are used. Although the flip angles of all 2DRF pulses are identical for the present approach, the spatial distribution of the excited magnetization still varies between different segments within the target volume (cf., e.g., Ref. 15). This also means that the longitudinal magnetization present prior to the next segment's excitation shows such a variation under non-fully-relaxed conditions that may yield a modulation of the resulting excitation profile. It should be emphasized that this holds for any acquisitions involving arbitrarily shaped profiles and segmented 2DRF excitations and is not specific to the signal scaling approach presented. To avoid this problem, one or two dummy shots could be performed for each 2DRF segment to establish a segment-specific steady state. In the case of performing several averages for a segment, it would be more efficient to acquire all averages of a segment in immediate succession once the segment-specific steady state has been achieved.

Upon discarding segments with very low B_1 weightings that provide only marginal signal contributions (typical flip angle of 0.2°), the acquisition time was reduced, but no significant effect on the profile resolution or signal amplitude was observed. It should be emphasized that such low weightings are more likely to be present at or around zero crossings of the weighting function rather than far out in k-space. For instance, two of the four segments for the gray matter profile discarded were in the inner half of the covered k-space range, while the eight outermost segments did not fall below the chosen threshold.

In this study, the calculation of the B_1 weighting was based on the low-flip-angle approximation in order to be able to be performed on-the-fly, which would be very useful for routine applications. However, this approach also limited the maximum flip angles applicable without significant profile distortions to about 50°. To be able to use larger flip angles, more elaborate RF pulse design algorithms (e.g., Refs. 22–24) are required. This likely includes both nonlinear designs of the 2DRF pulse, as well as nonlinear transformations of individual segments when scaling up to α_{max}.

If shorter echo times are desirable, the refocusing RF pulse that eliminates the unwanted side excitations could be removed. In this case, the excitation pulse must be designed such that the side excitations appear outside of the object to avoid unwanted signal contamination. This requires a larger field-of-excitation, i.e., a denser sampling in the blip direction, which means that more lines and 2DRF segments are needed.

CONCLUSIONS

Signal scaling combined with weighted averaging can increase the SNR of measurements with segmented 2D-selective RF excitations considerably. Thus, it could help to overcome limitations in single-voxel MRS measurements of tailored target regions, particularly for highly segmented 2D RF excitations.

Acknowledgments

Grant sponsor: Deutsche Forschungsgemeinschaft; Grant number: FI 1544/1; Grant sponsor: Bundesministerium für Bildung und Forschung (Neuroimage Nord).

References

1. Bottomley PA, Hardy CJ. Two-dimensional spatially selective spin inversion and spin-echo refocusing with a single nuclear magnetic resonance pulse. J Appl Phys. 1987; 62:4284–4290.
2. Hardy CJ, Cline HE. Spatial localization in two dimensions using NMR designer pulses. J Magn Reson. 1989; 82:647–654.
3. Pauly J, Nishimura D, Macovski A. A k-space analysis of small-tip-angle excitations. J Magn Reson. 1989; 81:43–56.
4. Börnert P, Schäffter T. Curved slice imaging. Magn Reson Med. 1996; 36:932–939. [PubMed: 8946359]
5. Rieseberg S, Frahm J, Finsterbusch J. Two-dimensional spatially selective RF excitation pulses in echo-planar imaging. Magn Reson Med. 2002; 47:1186–1193. [PubMed: 12111965]
6. Saritas EU, Cunningham CH, Lee JH, Han ET, Nishimura DG. DWI of the spinal cord with reduced FOV single-shot EPI. Magn Reson Med. 2008; 60:468–473. [PubMed: 18666126]
7. Finsterbusch J. Fast-spin-echo imaging of inner fields-of-view with 2D-selective RF excitations. J Magn Reson Imaging. 2010; 31:1530–1537. [PubMed: 20512911]
8. Sung K, Nayak KS. B1+ compensation in 3T cardiac imaging using short 2DRF pulses. Magn Reson Med. 2008; 59:441–446. [PubMed: 18219634]
9. Qin Q, Gore JC, Does MD, Avison JM, de Graaf RA. 2D arbitrary shape selective excitation summed spectroscopy (ASSESS). Magn Reson Med. 2007; 58:19–26. [PubMed: 17659614]
10. Busch MG, Finsterbusch J. Spatially 2D-selective RF excitations using the PROPELLER trajectory: basic principles and application to MR spectroscopy of irregularly shaped single voxel. Magn Reson Med. 2011; 66:1218–1225. [PubMed: 21465546]

11. Snyder J, Haas M, Dragonu I, Hennig J, Zaitsev M. Three-dimensional arbitrary voxel shapes in spectroscopy with submillisecond TEs. NMR Biomed. 2012; 25:1000–1006. [PubMed: 22290622]
12. Hardy CJ, Bottomley PA. ^{31}P spectroscopic localization using pinwheel NMR excitation pulses. Magn Reson Med. 1991; 17:315–327. [PubMed: 2062206]
13. Panych LP, Oshio K. Selection of high-definition 2D virtual profiles with multiple RF pulse excitations along interleaved echo-planar k-space trajectories. Magn Reson Med. 1999; 41:224–229. [PubMed: 10080266]
14. Weber-Fahr W, Busch MG, Finsterbusch J. Short-echo-time MR spectroscopy of single voxel with arbitrary shape in the living human brain using segmented 2D-selective RF excitations based on a blipped-planar trajectory. Magn Reson Imaging. 2009; 27:664–671. [PubMed: 19108976]
15. Finsterbusch J, Busch MG. Segmented 2D-selective RF excitations with weighted averaging and flip angle adaptation for MR spectroscopy of irregularly shaped voxel. Magn Reson Med. 2011; 66:333–340. [PubMed: 21360589]
16. Conolly S, Nishimura D, Macovski A, Glover G. Variable-rate selective excitation. J Magn Reson. 1988; 78:440–458.
17. Hargreaves BA, Cunningham CH, Nishimura DG, Conolly SM. Variable-rate selective excitation for rapid MRI sequences. Magn Reson Med. 2004; 52:590–597. [PubMed: 15334579]
18. Larson, PE.; Kerr, AB.; Pauly, JM.; Vigneron, DB. Constant time VERSE for RF amplitude reduction in spectral-spatial pulses with improved time robustness. Proceedings of the 16th Annual Meeting of ISMRM; Toronto, Canada. 2008. p. 3140
19. Bottomley PA. Spatial localization in NMR spectroscopy *in vivo*. Ann NY Acad Sci. 1987; 508:333–348. [PubMed: 3326459]
20. Provencher SW. Estimation of metabolite concentrations from localized in vivo proton NMR spectra. Magn Reson Med. 1993; 30:672–679. [PubMed: 8139448]
21. Hardy CJ, Cline HE, Bottomley PA. Correcting for nonuniform k-space sampling in two-dimensional NMR selective excitation. J Magn Reson. 1990; 87:639–645.
22. Shinnar M, Bolinger L, Leigh JS. The synthesis of soft pulses with a specified frequency response. Magn Reson Med. 1989; 12:88–92. [PubMed: 2607965]
23. Pauly J, Le Roux P, Nishimura D, Macovski A. Parameter relations for the Shinnar-Le Roux selective excitation pulse design algorithm. IEEE Trans Med Imaging. 1991; 10:53–65. [PubMed: 18222800]
24. Pauly JM, Spielman D, Macovski A. Echo-planar spin-echo and inversion pulses. Magn Reson Med. 1993; 29:776–782. [PubMed: 8350720]

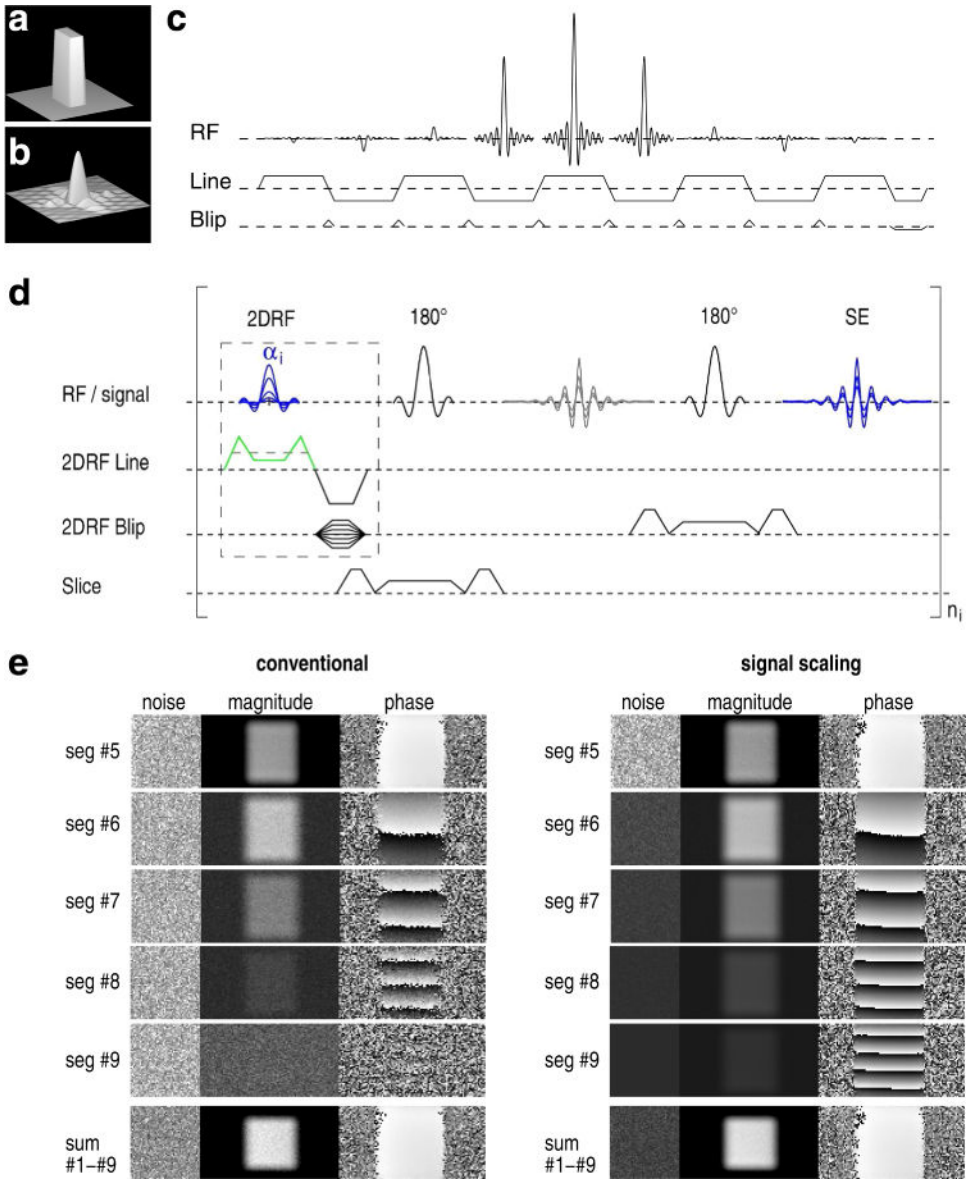

FIG. 1.

a–c: Example for a 2DRF pulse based on a blipped-planar trajectory that excites a rectangular profile. **a:** Desired rectangular excitation profile, **b:** its Fourier transformation, and **c:** the corresponding 2DRF excitation for a nine-line blipped-planar trajectory. The RF envelope of each line has a sinc shape, but their relative amplitudes differ. **d:** PRESS sequence for single-voxel MR spectroscopy using single-line segments of the 2DRF excitation shown in (c). The gradient amplitude is decreased in the center of the 2DRF segment (green) to reduce the RF peak amplitude. **e:** Excitation profiles (image resolution $2.0 \times 2.0\ mm^2$) of five of the nine single-line segments (profile size $35 \times 35\ mm^2$, resolution 5 mm) and of the sum of all segments obtained with the conventional experiment (left) and the proposed signal scaling approach (right) for nine acquisitions, i.e., one per segment. For the sake of clarity, the segments #1–#4 are not shown, because they differ from the segments #9–#5 only by the polarity of the phase gradient. Gray scalings do not differ between the

conventional and the signal scaling data for the individual segments and the sum. It should be emphasized that the shape of the RF envelope and the magnitude profiles, in general, vary between the different lines for nonrectangular profiles. [Color figure can be viewed in the online issue, which is available at wileyonlinelibrary.com.]

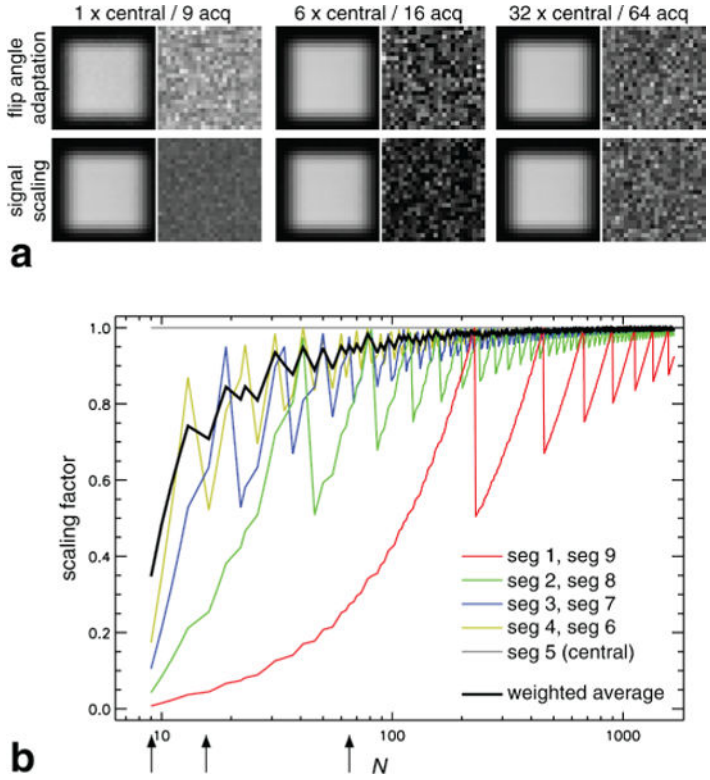

FIG. 2.

a: MR images of a rectangular profile (35 × 35 mm^2, resolution 5 mm) obtained with nine single-line 2DRF segments (cf. Fig. 1e) using flip angle adaptation and signal scaling. The target excitation and a background noise region are shown. Note that the image intensities were scaled with the number of averages of the central segment to obtain comparable intensities (identical gray scaling for the signal regions). The gray scaling of the noise region was identical between flip angle adaptation and signal scaling but was adapted to the number of acquisitions, because the noise intensity varied by a factor of 15. **b:** Plots of the individual scaling factors and their weighted average (f_{sum}) vs. the total number of acquisitions N for the nine single-line 2DRF segments (rectangular profile, 35 × 35 mm^2, resolution 5 mm) as used in Fig. 1e and (a). The arrows in (b) indicate the N used for the examples shown in (a). See text for details.

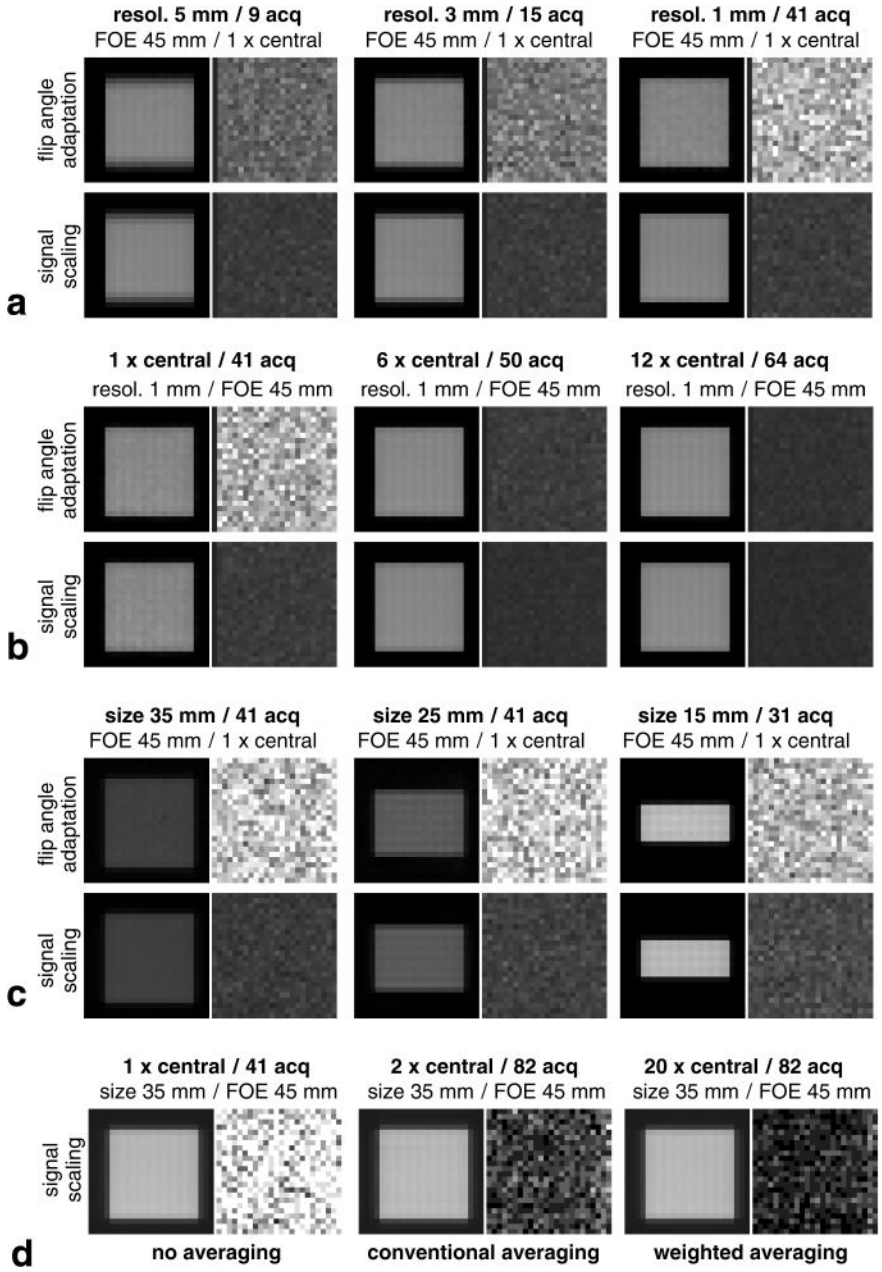

FIG. 3.

MR images of rectangular profiles obtained with segmented 2DRF excitations for different profile and 2DRF parameters. The target excitation and a background noise region are shown. **a:** Variation of the 2DRF's resolution (profile size 35 × 35 mm^2). **b:** Variation of the number of acquisitions (profile size 35 × 35 mm^2). Note that the images were scaled with the number of averages of the central segment to obtain comparable intensities. **c:** Variation of the profile size in the blip direction, where the size in the line direction was fixed to 35 mm (resolution 1 mm). **d:** Measurements with signal scaling for no averaging (left), conventional averaging (middle), and weighted averaging (right). The 2DRF resolution was 1 mm. Note that the images were scaled with the number of averages of the central segment

to obtain comparable intensities. The gray scalings for all noise and all signal regions are identical in each subfigure, respectively, which means that different intensities directly represent different noise levels and signal amplitudes. See text for details.

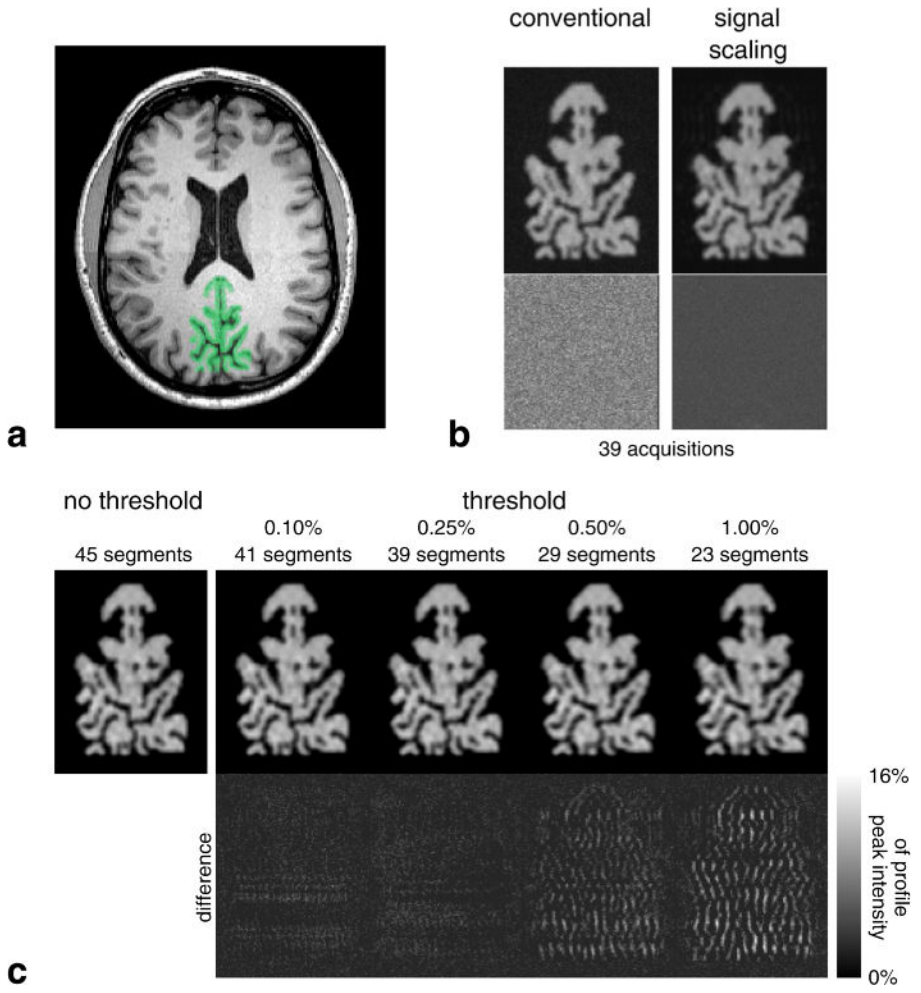

FIG. 4.

a: Anatomically defined 2D target profile (resolution 1 mm, size 35 × 54 mm^2) covering parietal gray matter of a healthy volunteer overlaid on a T_1-weighted acquisition (in-plane resolution 1.0 × 1.0 mm^2). **b:** Corresponding excitation profiles and background noise acquired in a phantom without (left) and with signal scaling (right) for one average per segment. **c:** Influence of thresholding low B_1 weighting segments on the excitation profile. The difference images are relative to the acquisition without thresholding. The gray scale bars refer to the peak intensity observed for the profile without thresholding. The profiles were acquired with an in-plane resolution of 0.5 × 0.5 mm^2. See text for details.

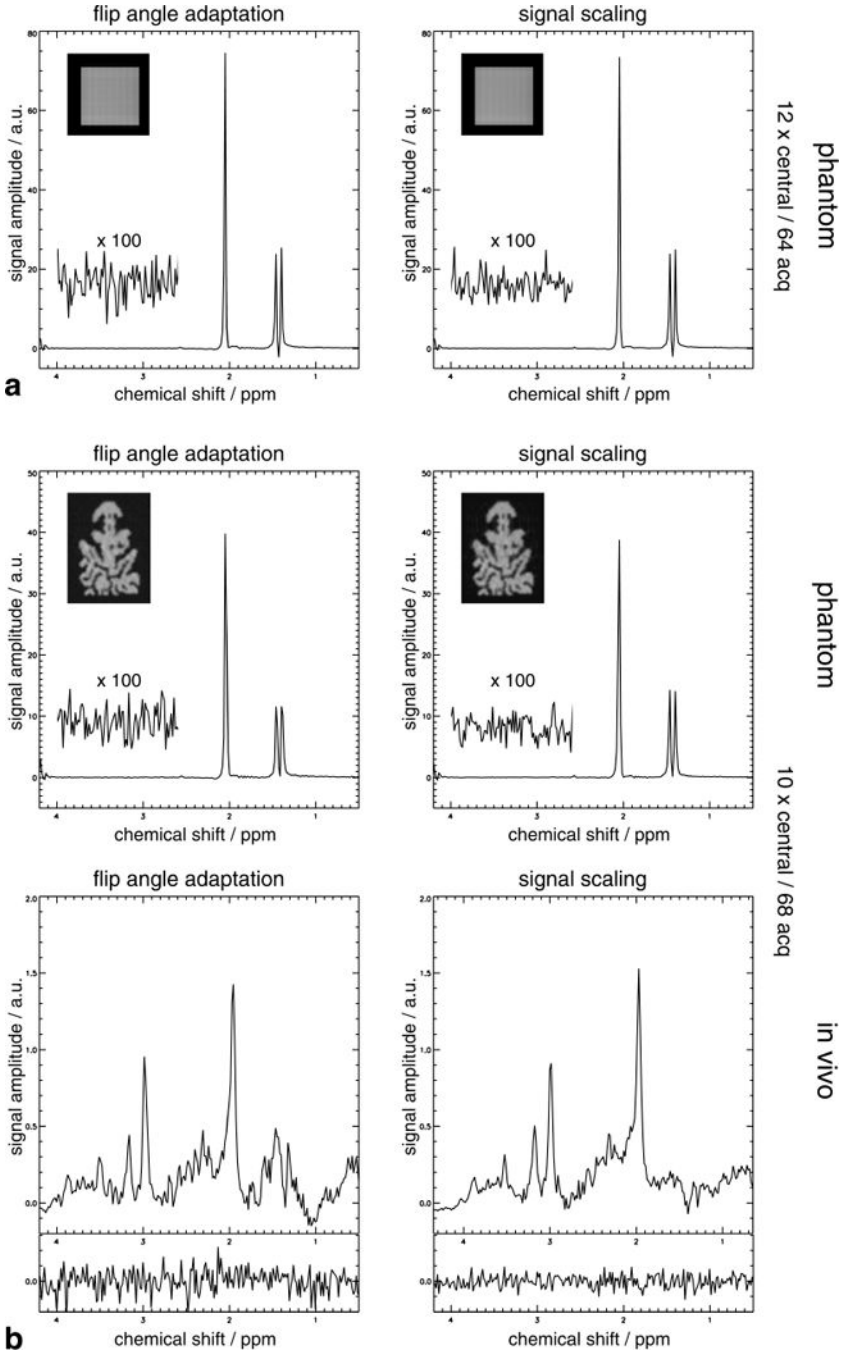

FIG. 5.

Results of the phantom and in vivo single-voxel MRS measurements for **(a)** a rectangular excitation profile (size 35 × 35 mm^2, resolution 1 mm, 64 acquisitions) and **(b)** the gray matter profile (size 35 × 54 mm^2, resolution 1 mm, 68 acquisitions) from Fig. 4 acquired with flip angle adaptation and signal scaling. The inlet images present excitation profiles acquired in a phantom with an in-plane resolution of 0.5 × 0.5 mm^2. For the phantom experiments, a frequency range in which no signal is expected is amplified to visualize the noise level. For the in vivo measurements, noise-only acquisitions are shown below the

spectra that were obtained by turning off all RF pulses. For signal scaling, the noise level is reduced between 35 and 40% across these experiments. See text for details.